JOURNAL OF GEOPHYSICAL RESEARCH, VOL. 112, A06325, doi:10.1029/2006JA012146, 2007

Coordinated optical and radar observations of ionospheric pumping for a frequency pass through the second electron gyroharmonic at HAARP

M. J. Kosch,[1,2,3] T. Pedersen,[1] E. Mishin,[4] S. Oyama,[5,6] J. Hughes,[7] A. Senior,[2] B. Watkins,[5] and B. Bristow[5]

Received 30 October 2006; revised 20 January 2007; accepted 12 February 2007; published 23 June 2007.

[1] On 4 February 2005, the High-frequency Active Auroral Research Program (HAARP) facility was operated in O and X mode while pointing into the magnetic zenith to produce artificial optical emissions in the ionospheric F layer. The pump frequency was set to 2.85 MHz to ensure passing through the second electron gyroharmonic of the decaying ionosphere. Optical recordings at 557.7 and 630 nm were performed simultaneously with the side-viewing high frequency (HF) and colocated ultra high frequency (UHF) ionospheric radars. No X-mode effects were found. For O-mode pumping, when passing from below to above the second gyroharmonic frequency, the optical intensity shows a distinct increase when the plasma frequency passes through the second electron gyroharmonic, while the UHF backscatter changes from persistent to overshoot in character. The optical intensity decreases when pump wave reflection ceases, dropping to zero when upper-hybrid resonance ceases. The HF radar backscatter increases when the upper-hybrid resonance frequency passes from below to above the second gyroharmonic frequency. These observations are consistent with the coexistence of the parametric decay and thermal parametric instabilities above the second gyroharmonic. The combined optical and radar data provide evidence that up to three electron-acceleration mechanisms are acting, sometimes simultaneously, depending on the pump frequency relative to the second gyroharmonic. In addition, we provide the first evidence of lower-hybrid waves in HF radar centerline data and show that the parametric decay instability producing Langmuir waves can be stimulated in the magnetic zenith at high latitudes despite the pump wave not reaching the nominal frequency-matching height.

Citation: Kosch, M. J., T. Pedersen, E. Mishin, S. Oyama, J. Hughes, A. Senior, B. Watkins, and B. Bristow (2007), Coordinated optical and radar observations of ionospheric pumping for a frequency pass through the second electron gyroharmonic at HAARP, *J. Geophys. Res.*, *112*, A06325, doi:10.1029/2006JA012146.

1. Introduction

[2] Pumping the ionosphere with high-power high-frequency (HF) radio waves, typically in the range 2–10 MHz, can induce several instabilities, which result in electron acceleration. These electrons excite the neutral atmospheric constituents by collisions. A fraction of this energy is released as photons with wavelengths identical to the natural auroras. The most easily observed artificial optical emissions are O(^{1}D) 630 nm and O(^{1}S) 557.7 nm, with thresholds of ~2 and ~4.2 eV, respectively, although the effective threshold for O(^{1}D) is ~3.5 eV because of the presence of N_2 [*Haslett and Megill*, 1974]. The phenomenon has been known at mid- and low latitudes since the 1970s; however, it has only been unambiguously observed at high latitudes fairly recently, notably at the European Incoherent Scatter facility (EISCAT, 69.59°N, 19.23°E) in Norway [*Brändström et al.*, 1999] and at the High-Frequency Active Auroral Research Program facility (HAARP, 62.39°N, 145.15°W) in Alaska [*Pedersen and Carlson*, 2001]. Controlled experiments, such as described below, are important for understanding natural electron acceleration and precipitation processes [e.g., *Samara et al.*, 2004] as well as testing wave-plasma interaction theories. In addition, the optical observations during ionospheric pumping experiments give information about the neutrals [e.g., *Gustavsson et al.*, 2001] as well as reveal the energy spectrum of the accelerated electrons [*Gustavsson et al.*, 2005].

[1]Space Vehicles Directorate, Air Force Research Laboratory, Hanscom AFB, Bedford, Massachusetts, USA.
[2]Communication Systems, Lancaster University, Lancaster, UK.
[3]Honorary Research Fellow, University of Kwazulu-Natal, Durban, South Africa.
[4]Institute for Scientific Research, Boston College, Chestnut Hill, Massachusetts, USA.
[5]Geophysical Institute, University of Alaska, Fairbanks, Alaska, USA.
[6]Solar-Terrestrial Environment Laboratory, Nagoya University, Nagoya, Japan.
[7]Physical Sciences, Embry-Riddle Aeronautical University, Daytona Beach, Florida, USA.

0148-0227/07/2006JA012146$09.00

[3] EISCAT has two colocated incoherent scatter radars, which observe the pump-induced electron Langmuir (L) and ion-acoustic waves (IA) as well as allow measurement of artificial electron- and ion-temperature enhancements. These show electron- and ion-temperature enhancements up to ~4000 K and ~500 K, respectively [*Rietveld et al.*, 2003]. Colocated at HAARP is the Modular UHF Ionospheric Radar (MUIR) [*Oyama et al.*, 2006], which is capable of observing the pump-induced L and IA waves but not the incoherent scatter spectrum without several minutes of integration. Hence extracting ion and electron temperatures with integration times of seconds is not possible at HAARP. Both facilities have well located Super Dual Auroral Radar Network (SuperDARN) HF radars [Kodiak for HAARP and Cooperative UK Twin Located Auroral Sounding System (CUTLASS) for EISCAT], capable of observing field-aligned plasma irregularities, called striations, which are symbiotic with upper-hybrid (UH) electrostatic waves [e.g., *Kosch et al.*, 2002a, 2002b; *Hughes et al.*, 2003, 2004], as well as various optical instruments.

[4] Most ionospheric modification phenomena are sensitive to the pump frequency relative to multiples (n) of the electron gyrofrequency, and these have been extensively tested for $n \geq 3$ [e.g., *Kosch et al.*, 2005]. HAARP is able to pump the ionosphere on the second electron gyroharmonic (GH) [e.g., *Djuth et al.*, 2005], which has produced some unique features [*Kosch et al.*, 2005; *Mishin et al.*, 2005a] described below. HF and ultra high frequency (UHF) radar, as well as optical, observations for a pump frequency pass through the second GH are the primary focus here, improving upon the first attempt which was limited to optical data only [*Kosch et al.*, 2005].

[5] Generally, there are three main resonant wave interactions that occur for O-mode electromagnetic wave (EM_O) pumping of the ionospheric plasma [e.g., *Mishin et al.*, 2005a], all resulting in electron acceleration. First, near the HF pump reflection level where the pump and plasma frequencies match, L and IA waves may be produced by either parametric decay (PDI_L), $EM_O \rightarrow L + IA$, or the oscillating two-stream instabilities ($OTSI_L$), i.e., $EM_O \rightarrow L + \delta n_e$, where density irregularities are denoted by δn_e. Usually, PDI_L and $OTSI_L$ are associated with weak and strong plasma turbulence, respectively [e.g., *Fejer*, 1979]. These electrostatic plasma waves (L and IA) propagate near-parallel to the magnetic field direction. Both IA and L waves are routinely detected by UHF or very-high-frequency (VHF) radars colocated with the HF pump wave source as ion- or plasma-line backscatter enhancements, respectively. This mechanism is fast acting (<10 ms) [e.g., *Djuth et al.*, 2004].

[6] For magnetic zenith (MZ) injections, i.e., zenith angle $\chi \sim 13°$ at EISCAT and $\chi \sim 15°$ at HAARP (where χ is the magnetic field zenith angle), which are outside the Spitze cone ($\chi \sim 6°$ at EISCAT and $\chi \sim 8°$ at HAARP), the pump waves refract down in altitude [e.g., *Kosch et al.*, 2002a], thereby lowering the reflection altitude. The large frequency mismatch [see e.g., *DuBois et al.*, 1993] makes $OTSI_L$ development practically impossible by requiring an unrealistically high pump power. However, UHF radar observations do show significant plasma- and ion-line backscatter enhancements [*Ashrafi et al.*, 2007; *Dhillon and Robinson*, 2005; *Oyama et al.*, 2006]. *Gurevich et al.* [1999, 2002] suggested that pump-induced striations would allow frequency matching for PDI_L outside the Spitze cone to occur owing to ducting of the pump wave inside the plasma depletions. *Mishin et al.* [2001] noted that, since the zenith angle of the magnetic field at high latitudes is small, a significant field-parallel component of the pump-wave electric field vector is present in the region of downward refraction. Furthermore, the matching condition for PDI_L can be achieved outside the Spitze cone (see below). Simultaneous observations of SuperDARN HF radar backscatter from striations and EISCAT UHF radar ion-line enhancements, along with artificial optical emissions, provide evidence of Langmuir turbulence in the MZ outside the Spitze cone at high latitude (*Ashrafi et al.*, 2007) Here we provide further evidence for the PDI_L mechanism for pumping in the MZ outside the Spitze cone at HAARP, in conjunction with optical observations, and estimate the maximum zenith angle for which this may occur.

[7] Second, UH and electron Bernstein (EB) electrostatic waves coupled to lower hybrid (LH) waves may be produced by parametric decay ($PDI_{UH/EB}$) of the pump wave, i.e., $EM_O \rightarrow UH/EB + LH$ [e.g., *Istomin and Leyser*, 1995]. The UH/EB and LH electrostatic waves propagate near-perpendicular to the magnetic field line. Whether UH or EB waves are excited depends on the dispersion characteristics of the plasma wave associated with the pump frequency used. This mechanism is rapid (<10 ms) and has a low threshold of excitation [e.g., *Mishin et al.*, 2005a]. $PDI_{UH/EB}$ can occur anywhere where suitable local ionospheric conditions exist, including in the MZ outside the Spitze cone and in a nominally underdense ionosphere [*Mishin et al.*, 2005b]. Significantly for producing artificial optical emissions, the collapse of field-aligned LH wave plasma density cavities causes electron acceleration along the magnetic field line by Landau damping [*Musher et al.*, 1978; *Mishin et al.*, 2004].

[8] Natural LH waves are known to occur in the topside auroral ionosphere and have been observed by rockets [*Vago et al.*, 1992] and low-altitude satellites [*Kjus et al.*, 1998]. These waves are mostly associated with field-aligned plasma density depletions, the collapse of which results in particle acceleration [*Robinson et al.*, 1996a, 1996b]. The LH wave frequency in the ionosphere is ~8 kHz. Pump-induced UH/EB waves have been observed directly by the Kodiak SuperDARN HF radar [*Hughes et al.*, 2003, 2004], but no evidence for LH waves have been published. *Mishin et al.* [2004] provided evidence that this mechanism exists based on the rapid optical response at pump on, although there is ambiguity with the PDI_L mechanism described earlier. In addition, *Kuo et al.* [1997] showed that UH waves can excite short-scale oblique L waves via the oscillating two-stream instability of the primary UH waves ($OTSI_{UH}$). Nonlinear interactions then result in rapid wave-spectrum broadening of the L waves [*Mishin et al.*, 2004]. Despite the modest output power at low pump frequencies (e.g., 2.85 MHz), the threshold for $PDI_{UH/EB}$ can be exceeded at HAARP [*Mishin et al.*, 2004]. Here we provide evidence for $PDI_{UH/EB}$ mechanism, as well as for LH waves in SuperDARN radar centerline data for the first time, in conjunction with optical observations.

[9] Third, UH waves may be generated by the thermal parametric instability (TPI_{UH}) [e.g., *Grach et al.*, 1981; *Dysthe et al.*, 1982]. The electromagnetic pump wave (f_O) is converted into UH electrostatic waves (f_{UH}) on naturally occurring magnetic field-aligned plasma density irregularities (called striations) for $f_O = f_{UH} = \sqrt{f_P^2 + f_C^2}$, where f_P is the local plasma frequency ($f_P \simeq 9\sqrt{n_e}$ kHz, n_e is the plasma density in cm^{-3}), and f_C is the local electron gyrofrequency which is proportional to magnetic-field strength. The UH plasma waves propagate near-perpendicular to the magnetic field direction and can be trapped within the meter-scale striations, heating the plasma further, causing further depletion and trapping on a timescale of several seconds in a positive feedback cycle [*Grach et al.*, 1981; *Dysthe et al.*, 1982], i.e., $EM_O \rightarrow UH + \delta n_e$. Whenever significant background meter-scale density irregularities are present, the so-called resonance instability develops where the magnitudes of the waves and striations grow explosively [*Vaskov and Gurevich*, 1977].

[10] The UH resonance altitude (H_{UHR}) is typically a few (3–8) km below the HF reflection altitude (H_O where $f_O = f_P$). Hence the cone where TPI_{UH} is possible is greater than the Spitze cone. The TPI_{UH} cone size is a function of the HF pump wave refraction, which depends on the pump frequency and electron-density height profile. *Mishin et al.* [2005b] showed that for MZ pointing, pumping below $f_C/\sin\chi \approx 5.5$ and ≈ 6.3 MHz at HAARP and EISCAT, respectively, would ensure that UH resonance would be reached. Since artificial optical emission experiments occur only at night when the ionosphere is weak, this pump-frequency limitation is of no practical consequence. Generally, the TPI_{UH} is easily stimulated in the MZ at HAARP and EISCAT, i.e., at high latitudes, even at low pump powers (<4 MW effective radiated power) [*Wright et al.*, 2006]. Meter-scale pump-enhanced striations are routinely observed by the SuperDARN radars and are clearly associated with artificial optical emissions [e.g., *Kosch et al.*, 2002a, 2002b]. EB waves are not trapped inside the striations and therefore do not contribute to TPI_{UH} [*Mjølhus*, 1993]. At pump on, it is common for an UHF radar to observe the $PDI_L/OTSI_L$ mechanism signature in the initial seconds until the TPI_{UH} mechanism takes over as the striations grow. This manifests itself as a strong ion-line (IA waves) or plasma-line (L waves) backscatter overshoot, which is subsequently quenched within seconds because of anomalous absorption on the striations [e.g., *Stubbe et al.*, 1994]. Fully established striations almost completely absorb the pump wave [*Stubbe*, 1996], thereby preventing $PDI_L/OTSI_L$, which can only occur above the UH resonance altitude [e.g., *Stubbe et al.*, 1994]. Here we provide evidence for the TPI_{UH} mechanism operating asymmetrically about the second GH.

[11] *Mishin et al.* [2005a] showed that both the TPI_{UH} and $PDI_{UH/EB}$ mechanisms could exist simultaneously for certain pump frequency regimes about the second GH, depending on the dispersion characteristics of the plasma waves, although they neglected the PDI_L mechanism. The ability to stimulate two mechanisms for electron acceleration provides an explanation for the unusually intense artificial optical emission observed when pumping near the second GH in the MZ at HAARP [*Kosch et al.*, 2005]. *Ashrafi et al.* [2007] also provided evidence for two simultaneous mechanisms by observing the simultaneous production of striations (TPI_{UH}) and IA waves ($EM_O \rightarrow L + IA$) when pumping near the fourth GH in the MZ at EISCAT. Here we provide evidence for up to three simultaneous electron acceleration mechanisms.

[12] Most ionospheric modification effects are sensitive to the pump frequency relative to the electron GH frequency [e.g., *Kosch et al.*, 2005]. For the third and higher GH, artificial optical emissions usually minimize [*Kosch et al.*, 2002b; *Gustavsson et al.*, 2006]. The growth of striations, and by association UH waves, are suppressed when pumping on the third or higher GH frequency [*Huang and Kuo*, 1994; *Honary et al.*, 1995; *Robinson et al.*, 1996a, 1996b]. *Huang and Kuo* [1994] and *Istomin and Leyser* [2003] predicted theoretically that UH waves and striations, and therefore also artificial optical emissions, would be stronger for pump frequencies just above a GH frequency compared to below it, i.e., an asymmetry would exist. By the same token, *Grach* [1979] and *Kuo and Rubinraut* [2005] have shown that efficient electron acceleration by UH waves generated via TPI_{UH} near $2f_C$ occurs just above the GH frequency. For both these effects, there is optical evidence [*Gustavsson et al.*, 2006; *Kosch et al.*, 2005] as well as SuperDARN radar evidence of striation intensity [*Kosch et al.*, 2002b], although the authors did not address this latter point directly. Here we provide further HF radar evidence of the asymmetry effect of the TPI_{UH} mechanism about the second GH.

[13] *Honary et al.* [1999] have shown that $PDI_L/OTSI_L$ persists when pumping on the third or higher GH frequency because the growth of striations is suppressed [e.g., *Ponomarenko et al.*, 1999; *Kosch et al.*, 2002b]. Hence the HF pump wave can reach the higher L wave matching height or near to it when pumping outside the Spitze cone without being dissipated at the lower UH resonance altitude by mode conversion into UH waves. Artificial optical emissions associated with persistent Langmuir turbulence on the fourth GH have been observed [*Ashrafi et al.*, 2007; *Kosch et al.*, 2004]. The colocated UHF radar (EISCAT) observed a persistent ion-line (IA waves) or plasma-line (L waves) backscatter enhancement throughout the pumping pulse. Since the pump GH frequency must be selected within kHz and the ionosphere is never stationary for long, it is practically difficult to prevent striation growth completely, although growth proceeds much more slowly. This manifests itself as a decline in UHF radar ion- or plasma-line backscatter power during the pump pulse. Here we provide UHF radar evidence of L waves for both suppressed and strong striation growth.

[14] The high electron temperatures (up to 4000 K) observed during pump-induced artificial optical emissions [*Rietveld et al.*, 2003] may account for a significant fraction of the $O(^1D)$ 630-nm emission [*Ashrafi et al.*, 2007] but can not account for the $O(^1S)$ 557.7-nm or other higher-threshold emissions [*Gustavsson et al.*, 2002]. Hence a significant but small fraction of the electrons must be accelerated to suprathermal energies [*Gustavsson et al.*, 2005]. To date, observations of pump-induced optical emissions are limited by the photon detection technology available and low (subvisual) optical intensities, hence most results focus on the steady state 630 nm emission,

which is partly due to the TPI_{UH} mechanism. Here we provide optical data down to new levels, i.e., a few Rayleighs.

[15] *Kosch et al.* [2005] have summarized past results from pumping near the second GH. Striations and UH waves, as observed by coherent radar backscatter, occurred [*Fialer*, 1974; *Minkoff et al.*, 1974] along with artificial optical emissions [*Sipler and Biondi*, 1972]. Coherent backscatter was enhanced [*Fialer*, 1974], and optical emissions become significantly brighter [*Haslett and Megill*, 1974] when the pump frequency happened to be close to the second GH. In addition, *Fialer* [1974] noted that coherent backscatter power, i.e., striations, maximized when pumping just above the second GH. This is consistent with optical observations about the second GH [*Kosch et al.*, 2005]. Here we provide further radar and optical evidence of this asymmetry effect.

[16] During the first pump frequency pass through the second GH in the MZ at HAARP, *Kosch et al.* [2005] and *Mishin et al.* [2005a] found several novel features. First, there was no minimum in the intensity of the artificial optical emissions, as is expected for higher GHs [*Kosch et al.*, 2002b; *Gustavsson et al.*, 2006]. Second, the intensity of the artificial optical emissions maximized for pump frequencies just above the second GH. The same trend is observed for higher GHs [*Gustavsson et al.*, 2006]. Third, the maximum in optical intensity was not associated with a change in electron energy spectrum, only flux. Fourth, the intensity of the 630 nm emission almost doubled when the plasma frequency at the pump-wave reflection altitude passed through the second GH, i.e., f_P ($H_{2f_{CO}}$) = $2f_{CO}$, and when the F-peak critical frequency passed through the second GH, i.e., $f_OF2 = 2f_C$ (H_{fOF2}). These observations suggest that L waves participated in cyclotron acceleration of electrons [*Mishin et al.*, 2005a]. In addition, optical emissions were produced for pump frequencies up to 400 kHz above the ionospheric critical frequency, consistent with *Pedersen et al.* [2003] and *Mishin et al.* [2005b], and irregular shaped optical structures, not necessarily in the pump beam center, appeared when pumping in this regime.

[17] Usually, when pumping into the MZ, an optical blob which is significantly smaller than the pump beam is produced [e.g., *Kosch et al.*, 2005; *Pedersen et al.*, 2003; *Rietveld et al.*, 2003]. *Djuth et al.* [2005] estimated the angular width of the optical blob at HAARP to be ~8° with a pump beam size of ~32 × 45°. *Pedersen et al.* [2003] found the average angular size to be ~7° for over 1000 images but for a variety of beam sizes. Attempts to observe striations using the Kodiak SuperDARN radar while pumping near the second GH failed [*Djuth et al.*, 2005; *Kosch et al.*, 2005], primarily because of propagation conditions not satisfying the backscatter orthogonality requirement at 10 MHz [*Kosch et al.*, 2005]. In addition, Djuth et al. and *Kosch et al.* [2005] had no means to observe L waves. Both these radar observational problems are successfully addressed here.

[18] The dispersion curves of the plasma electrostatic waves for pump frequencies around the second GH show that UH and EB plasma waves will exist above and below the second GH, respectively [*Grach*, 1979; *Mishin et al.*, 2005a]. This is significant because only UH waves are trapped in the density depletions of striations and contribute to the TPI_{UH} mechanism. Here we provide radar and optical evidence for this effect. *Fejer and Leer* [1972] suggested that EB waves might be excited by X-mode pumping. More specifically, *Das and Fejer* [1979] predicted theoretically that X-mode pumping on the second GH would produce striations. Our observations do not confirm this.

[19] Double resonance, i.e., the GH at UH resonance, occurs when $f_O = nf_C = f_{UHR}$, where f_O is known, nf_C is derived from the International Geomagnetic Reference Field (IGRF) model, and f_P is derived from ionosonde data. The threshold for TPI_{UH} decreases significantly, while the maximum growth rate increases close to this frequency regime [*Grach et al.*, 1994; *Norin et al.*, 2006]. As the HF reflection/refraction altitude increases for a fixed pump frequency in a decaying ionosphere after sunset, f_C decreases. Selecting the correct pump frequency in advance ensures that plasma resonance, i.e., $f_O = f_P$, and double resonance will be found, and a single pump frequency pass through the second GH will automatically be executed for both resonances.

[20] Stimulated electromagnetic emissions (SEE) are a common feature of ionospheric-pumping experiments. SEE spectral features provide many clues to the wave-plasma processes and have been extensively studied [e.g., *Leyser*, 2001]. Fundamentally, the SEE are due to the electromagnetic pump wave mode converting into electrostatic plasma waves, typically on density perturbations, and then reconverting back to electromagnetic waves after some interaction or cascade process, which propagate back down to the ground [e.g., *Carozzi et al.*, 2002]. The downshifted maximum (DM) is a common spectral feature for pump frequencies not on the third and higher GHs and is usually associated with UH wave-induced striations. The DM feature has been observed for pumping just below the second GH [*Djuth et al.*, 2005].

[21] This paper presents multiwavelength optical data and backscatter from two radar systems (section 2) along with their theoretical analysis (section 3) for pumping of the ionospheric plasma by high-power HF radio waves near the second GH.

2. Results

[22] On 4 February 2005, the HAARP facility was operated at 2.85 MHz between 03:00 and 05:50 UT immediately after sunset, with ~11 MW effective radiated power (ERP), corresponding to a beam size of ~32 × 45°, and pointing into the MZ (204° azimuth, 75° elevation). Starting at 03 UT, a pump modulation of 60 s off, 60 s O-mode, 60 s off, and 60 s X-mode was used to perform a single frequency pass through the second electron GH while searching for known O- and predicted X-mode resonances. Geomagnetic conditions were very quiet (Kp = 0).

[23] The colocated Digisonde provided ionospheric density profiles every 2 min in the range 1–6 MHz. The Kodiak SuperDARN radar [e.g., *Hughes et al.*, 2003, 2004], located ~650 km southwest of HAARP, was operating on beam 9 only, which overlooks HAARP, with 15 km range resolution and 1 s integration. The radar cycled through six frequencies (8.05, 9.35, 10.35, 11.55, 12.14, and 13.505 MHz) in order to ensure the best possibility for satisfying backscatter orthogonality conditions. The colocated 446 MHz MUIR [*Oyama et al.*, 2006], which had just been commissioned,

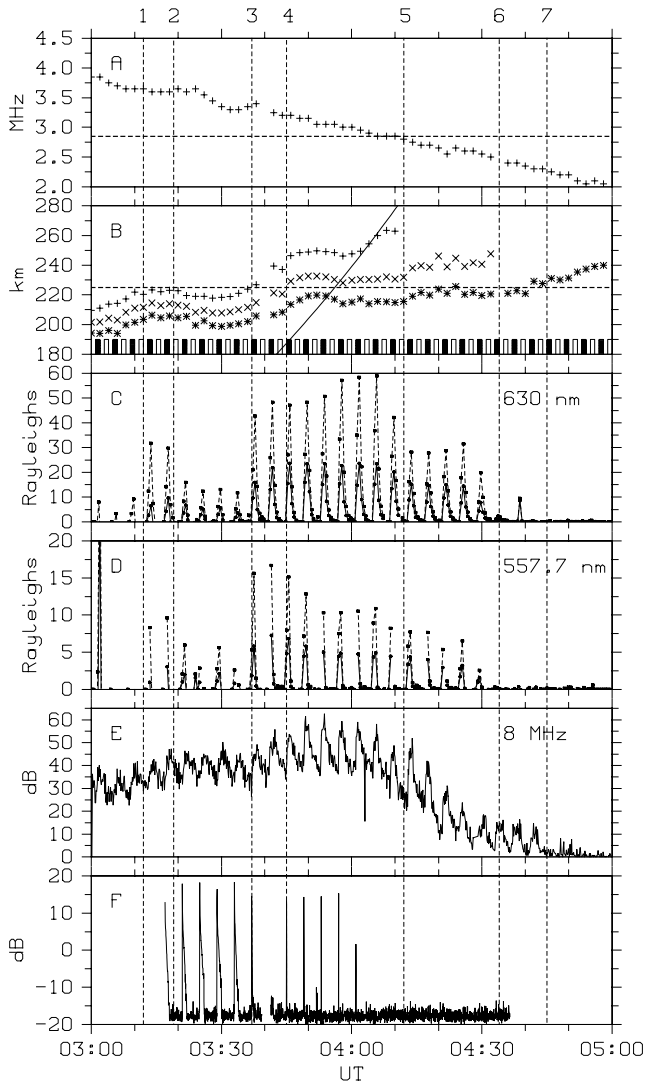

Figure 1. (a) The ionospheric critical frequency with time from colocated Digisonde data. The dashed horizontal line shows the pump frequency (2.85 MHz). (b) The O-mode reflection (positive sign), upper-hybrid resonance (multiplication sign), and X-mode reflection altitudes (asterisk) over HAARP at 2.85 MHz from Digisonde data. The dashed horizontal line is the altitude corresponding to the second electron gyroharmonic (~225 km). The solid diagonal line gives the solar terminator altitude. O- and X-mode pump pulses are denoted by the solid and unshaded bars. (c) The average background-subtracted 630 nm optical intensity in a ~20° (solid line) and ~2.5° (dashed line) cone about the HAARP beam center. (d) The average background-subtracted 557.7 nm optical intensity in a ~20° (solid line) and ~2.5° (dashed line) cone about the HAARP beam center. For Figures 1c and 1d, the dots give the start time of each 15 s integration, spaced 30 s apart. (e) HF radar backscatter power at 8 MHz. (f) UHF radar plasma-line backscatter power at 446 MHz. The labeled vertical dotted lines indicate significant times referred to in the text.

used a simple long-pulse transmission while recording plasma-line data on a single receiver channel only. The beam (−3 dB beam size ~8.6°) was pointing into the MZ with a transmitter pulse of 998 μs (~150 km), receiver gating of 10 μs (~1.5 km), and a data dump time of 10 ms. The upshifted plasma-line was observed from 03:17 to 03:39 UT, followed by downshifted plasma-line from 03:41 to 04:36 UT with a short data gap in between.

[24] All-sky optical recordings were performed by the colocated HAARP imager, alternating between the O(^{1}S) (557.7 nm) and O(^{1}D) (630 nm) emissions with 15 s integration, which were synchronized to start with 557.7 nm at each full minute. This gives a 557.7 (630) nm image integrated in the period 0–15 (15–30) s and 30–45 (45–60) s of each minute. Optical viewing conditions were ideal with clear sky, natural aurora on the far northern horizon only, and sunset twilight contamination on the western horizon.

[25] Figure 1 gives an overview of the observations. The labeled vertical dotted lines indicate significant times. Figure 1a shows the ionospheric critical frequency (f_oF2) from Digisonde data. The horizontal dashed line denotes pump frequency (2.85 MHz), which exceeded f_oF2 after ~04:12 UT (label 5). Figure 1b shows the O-mode reflection (positive sign), upper-hybrid resonance (multiplication sign), and X-mode reflection (asterisk) altitudes over HAARP at 2.85 MHz, also from Digisonde data. The dashed horizontal line at ~225 km altitude corresponds to the second electron GH as determined by the IGRF magnetic field model. The solid diagonal line gives the solar terminator altitude. O- and X-mode pump pulses are denoted by the solid and unshaded bars, respectively. Clearly, as time progresses, the HF reflection and UH resonance altitudes ascend. At ~03:45 UT (label 4), the UH resonance altitude passed through the second GH, i.e., the double resonance. At ~04:12 UT (label 5), the ionospheric O-mode critical frequency reached 2.85 MHz, corresponding to the solar terminator ascending through the F-region peak altitude. At ~04:34 UT (label 6), UH resonance ceased with X-mode reflection continuing to the end of the experiment. The Digisonde data are dominated by echoes from the local zenith, whereas HF pumping took place in the MZ some 60 km away in the F layer. Although not perfectly colocated, the measurement uncertainty introduced is expected to be smaller than that associated with scaling the ionograms, typically ±10 km [*Kosch et al.*, 2005].

[26] Figures 1c and 1d show the average background-subtracted and calibrated 630 and 557.7 nm optical intensity, respectively. The dashed and solid curves are for cones of ~2.5° and ~20° diameter centered on the MZ. The wide cone covers most of the artificially induced optical emissions, whereas the narrow cone covers the central bright spot within the artificially induced optical emission (see Figure 2, discussed below). Background subtraction is necessary because of the changing twilight illumination. The background was a piecewise linear fit to the data point at the end of each 4 min cycle, introducing an uncertainty of <0.5 R. The intrinsic noise level of the optical data is <1 R. The 630 nm optical intensity in the MZ (Figure 1c), peaking at ~58 R, is approximately double that averaged over much of the beam, peaking at ~24 R. The 557.7 nm emission is similar (Figure 1d), peaking at ~17 R in the MZ and ~7 R

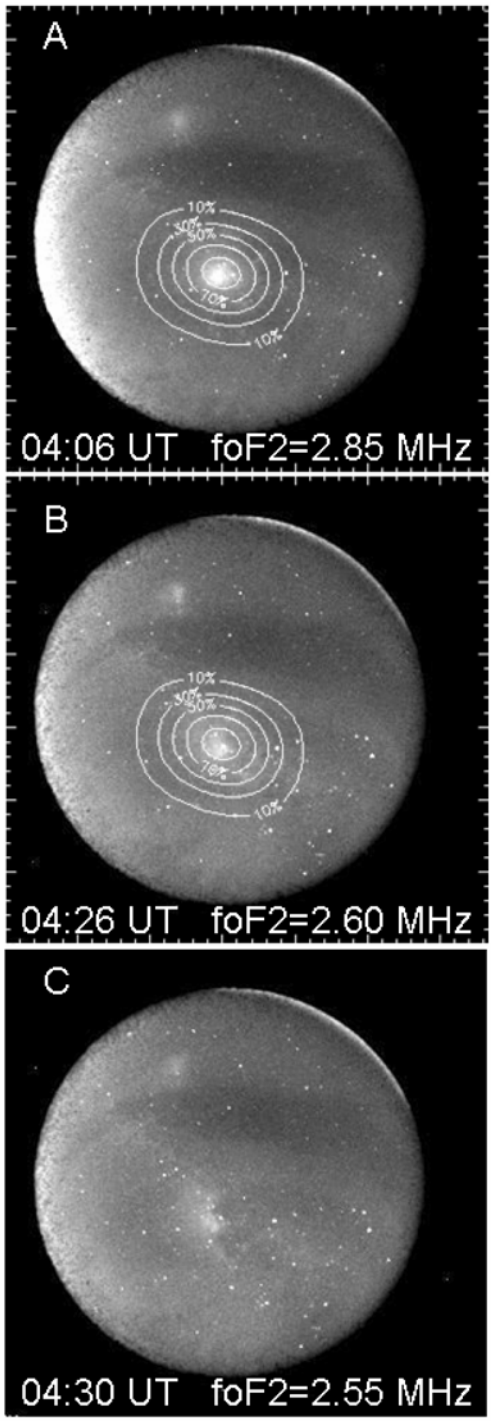

Figure 2. Example of 630 nm images of pump-induced artificial optical emissions from the HAARP all-sky imager with time and the ionospheric critical frequency overlaid. For all panels, north and east are to the top and right, respectively. The optical emissions on the western and northeastern horizon are due to sunset and natural aurora, respectively. The emission blob in the northwest is due to unrelated HIPAS heater operations. The spots correspond to stars. Figures 2a and 2b show percentage power contours from the HAARP beam.

over much of the beam. Clearly, both optical emissions are enhanced during the O-mode pump pulses. Camera saturation due to twilight renders the optical data useless prior to ~03:10 UT. No optical emissions are produced during the X-mode pump pulses. The single 630 nm pulse at ~04:39 UT during X-mode pumping is the result of man-made light contamination.

[27] The 630 nm emission provides clear evidence of electron heating, whereas the 557.7 nm emission provides clear evidence of suprathermal electron acceleration [*Gustavsson et al.*, 2002]. Since 60 s pumping is not long enough to ensure that the 630 nm emission reaches full saturation in the F layer [e.g., *Gustavsson et al.*, 2001], the intensity ratio $I(5577)/I(6300)$, which is an indicator of electron energy [*Gustavsson et al.*, 2002], is not presented here. The artificial optical emissions centered on the MZ continued until ~04:30 UT, which is well after HF reflection nominally ceased (~04:12 UT, label 5). At 04:30 UT, f_oF2 = 2.55 MHz, 300 kHz below the pump frequency. Optical emissions with an irregular structure were produced after 04:30 until ~04:38 UT. At 04:38 UT, when the irregular optical emissions ceased, f_oF2 = 2.4 MHz, 450 kHz below the pump frequency. Both these observations are consistent with the studies of *Kosch et al.* [2005] and *Pedersen et al.* [2003]. Since the irregular structures do not necessarily appear centered in the pump beam, they do not show well in Figures 1c and 1d.

[28] Figure 2 shows examples of 630 nm images of the pump-induced artificial optical emissions from the HAARP all-sky imager, with time and the ionospheric critical frequency overlaid. For all panels, north and east are to the top and right, respectively. The optical emissions on the western and northeastern horizon are due to sunset and natural aurora, respectively. The emission blob in the northwest is due to unrelated High-Power Auroral Stimulation (HIPAS) heater operations. The contours that correspond to percentage power of the HAARP beam are overlaid on Figures 2a and 2b. Figure 2a corresponds to when HF reflection and UH resonance were both possible. Figure 2b corresponds to UH resonance only being possible. Figure 2c shows an irregularly structured optical emission when UH resonance is close to ceasing. This image is similar to that of *Kosch et al.* [2005], who suggested that the pump beam was illuminating a random large-scale region in the ionosphere, dense enough to permit UH resonance. From a morphology point of view, Figures 2a and 2b are similar. The 630 nm optical emissions appear for >30% of maximum beam power, suggesting that ~3 MW ERP is the threshold for photon detection, consistent with the result of *Pedersen et al.* [2003] (~2 MW ERP). The central bright optical blob has an angular width of ~9° [*Kosch et al.*, 2007], consistent with *Djuth et al.* [2005] (~8°) and *Pedersen et al.* [2003] (~7°). Example of 557.7 nm images appear in the work of *Kosch et al.* [2007].

[29] Figure 1e shows the Kodiak radar backscatter power over HAARP for 8 MHz radar frequency. Clearly, backscatter power increases during the O-mode pump pulses, as expected. There is no clear evidence of irregularity production during the X-mode pump pulses. Unfortunately, the purity of the polarization could not be quantified (M. McCarrick, private communication). Hence O-mode leakage may account for the occasional apparent small

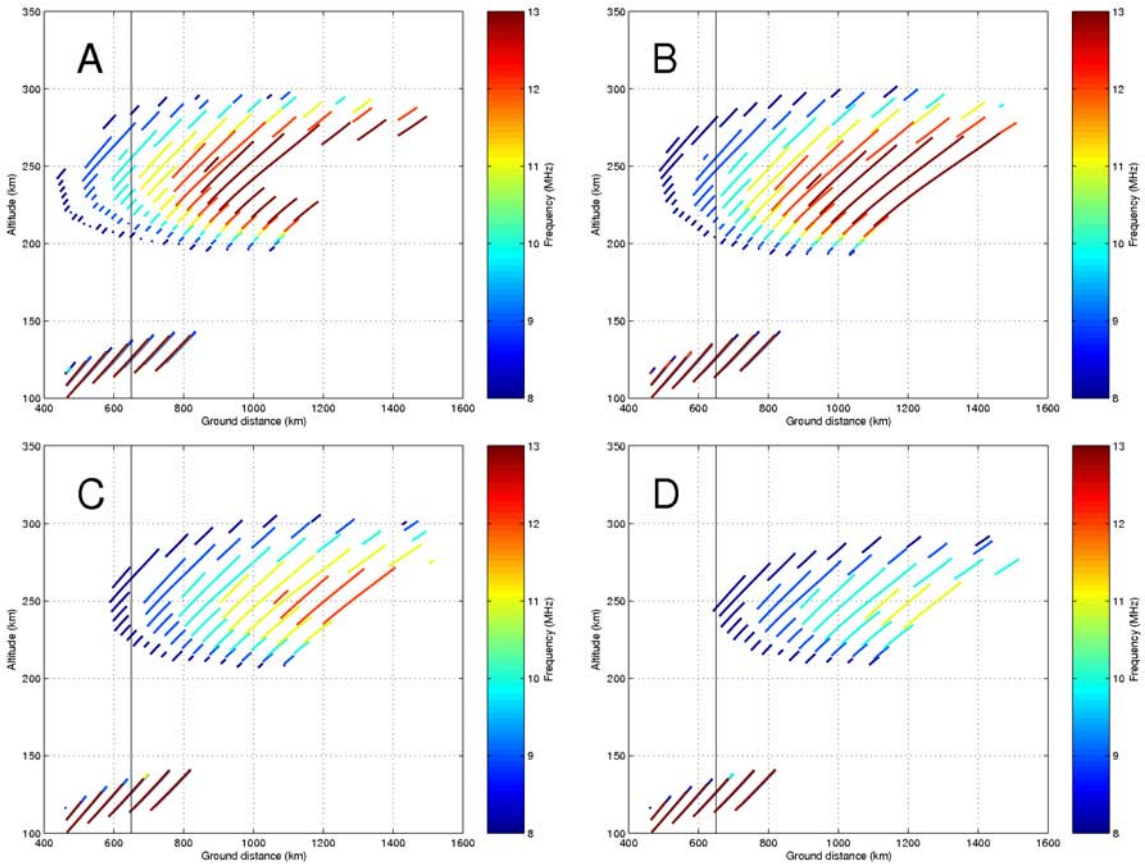

Figure 3. The intervals of the raypaths within 1° orthogonality to the magnetic field-line direction over HAARP are shown for the Kodiak radar beam 9 as a function of range, altitude, and frequency. HAARP's position is denoted by the vertical line. (a) 03:16, (b) 03:36, (c) 03:56, and (d) 04:16 UT.

increases in backscatter power during X-mode transmissions, or these may be due to natural irregularities. The nonzero background of backscatter power is a common feature at HAARP, resulting from natural plasma irregularities especially around sunset [*Djuth et al.*, 2005]. After ~04:20 UT, the average backscatter power enhancements decline, although pump-induced modulations are still clearly visible up to ~04:45 UT (label 7), consistent with the optical observations. Between ~03:45 and ~04:20 UT, the amplitude of the artificial backscatter enhancements is ~20–25 dB. For other times, this reduces to ~10–15 dB. We also note that prior to ~03:45 UT (label 4), the backscatter power data appear much noisier in character than after this time. Data from the higher SuperDARN radar frequencies are not shown, as they indicate the same results but lose orthogonality earlier during the experiment, as predicted by ray tracing.

[30] Figure 3 shows the intervals of the raypaths within 1° orthogonality to the magnetic field line direction over HAARP for the Kodiak radar beam 9 as a function of range, altitude, and frequency. The 6 Kodiak frequencies used are shown with different colors. HAARP's position is denoted by the vertical line, which also corresponds to the poleward −3 dB edge of the tilted pump beam. Figures 3a, 3b, 3c, and 3d show 03:16, 03:36, 03:56, and 04:16 UT, respectively. The ray trace takes into account the ionospheric tilt due to sunset by using ionosonde data from HAARP and King Salmon Island, which is near the Kodiak radar. It is obvious that F-region orthogonal backscatter persists the longest for the radar's lowest operating frequency. The general decline in radar backscatter power after ~04:10 UT also coincides with orthogonality coming from an ever-decreasing altitude range, ultimately becoming impossible. Orthogonal backscatter at 10 MHz ceases soon after 03:36 UT (Figure 3b), which is just prior to the pump frequency reaching the double resonance at ~03:45 UT. Assuming similar ionospheric propagation conditions, this explains why *Kosch et al.* [2005] were unsuccessful at observing SuperDARN backscatter during the first pump frequency pass through the second GH.

[31] Figure 1f shows the MUIR radar backscatter power in the MZ over HAARP. These data as well as the power spectral density have been presented by *Oyama et al.* [2006], but we interpret them here in the light of the optical and SuperDARN radar data (Figures 1c, 1d, and 1e). Within ~30 ms of pump on the backscatter, power increases during the O-mode pump pulses, as expected for the PDI_L mechanism [cf. *Isham et al.*, 1999]. There is no evidence of any effects during the X-mode pump pulses. The long transmitter pulse used (~1 ms) makes locating the altitude of the pump-induced backscatter echo difficult despite the receiver sampling at ~1.5 km resolution. However, estimates (not shown) are consistent with the Digisonde data. Prior to the double resonance (~03:45 UT, label 4), the MUIR back-

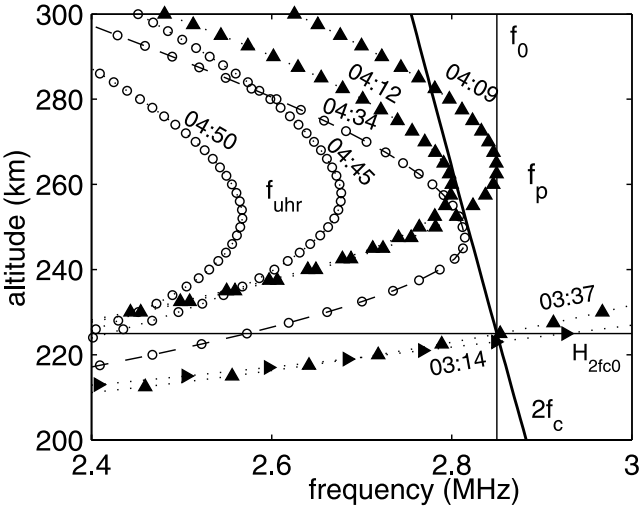

Figure 4. Height profiles of upper-hybrid resonance (f_{UHR}, open circles) and plasma frequency (f_P, solid triangles). The solid lines indicate second gyroharmonic frequency ($2f_C(H)$, diagonal), the pump frequency (f_O, vertical), and the height of the second gyroharmonic at the pump frequency used (H_{2fCO}, horizontal). Universal time for the different profiles is given as hh:mm.

scatter persists throughout the O-mode pump pulse, decreasing in strength with time. This indicates probable slow plasma irregularity growth. After ~03:45 UT (label 4), the MUIR backscatter is overshoot-like in character with only a brief impulse at the beginning of each O-mode pump pulse. This indicates strong striation growth associated with UH waves, consistent with the increased amplitude SuperDARN radar backscatter (Figure 1e). The change from upshifted to downshifted plasma-line observations at 03:39–03:41 UT means that one pump pulse is not observed. However, the physics of the observations are not affected, being the same for both up- and downshifted plasma-lines in the radar data. The timing of this technical change is unfortunate as it occurs between the plasma and double resonances (Figure 1, labels 3 and 4).

[32] Between ~04:15 and 04:40 UT, the X-mode reflection altitude approximately coincided with that for the second GH (Figure 1b, asterisk trace). No unambiguous evidence of any resonant effects were detected for the X-mode pump pulses, as were suggested by *Das and Fejer* [1979]. Experiments by one of us (M.J.K.) at EISCAT also produce negative results for X-mode pumping. Hence for discussion purposes, the HAARP pump cycle is effectively 1 min O-mode and 3 min off.

3. Discussion

[33] The vertical dashed lines in Figure 1 indicate important times: ~03:12–03:15 and ~03:37 UT (labels 1–3) when the altitude of HF reflection (H_O) coincided, or almost coincided, with that of the local second gyroharmonic, i.e., $f_P(H_O) \approx 2f_C(H_O)$ (plasma resonance), ~03:45 UT (label 4) when $H_{UHR} = H_{2f_{CO}}$ (double resonance), ~04:12 UT (label 5) when nominal HF reflection ceased, ~04:34 UT (label 6) when the UH resonance (UHR) ceased, and ~04:45 UT (label 7) when HF backscatter and artificial optical emissions ceased. The intensity of the O(^{1}D) and O(^{1}S) optical emissions, I(6300) and I(5577) respectively, tripled in the MZ when plasma resonance was almost reached at ~03:12 UT (label 1). After ~03:15 UT (label 2), when the plasma density temporarily increased so that $f_P(H_O) < 2f_C(H_O)$, both I(6300) and I(5577) decreased. When the plasma resonance was reached at ~03:37 UT (label 3), both I(6300) and I(5577) almost quadrupled, only reducing at ~04:12 UT (label 5) when the steadily decreasing f_oF2 dropped below the pump frequency f_o = 2.85 MHz.

[34] Figure 4 shows the frequency-height plots introduced by *Mishin et al.* [2005a]. The local UH resonance frequency (f_{UHR}, circles), local plasma frequency (f_P, triangles), and local second gyroharmonic frequency ($2f_C$, solid line) are shown as a function of height (H) as determined from ionosonde profiles and the IGRF model. Comparing Figures 1 and 4 shows that I(6300) decreased by ~10 R (~30%) when f_oF2 decreased below $2f_C(H_{foF2})$ after ~04:12 UT. Also, prior to the cessation of the I(6300) emission, the line $2f_C(H)$ intersected the weakening $f_{UHR}(H)$ at ~04:34 UT for the last time. However, the pump-induced enhancements in the HF radar backscatter power (Figure 1e) are clearly visible up to ~04:45 UT (label 7). These are associated with the irregularly shaped optical emissions (see Figure 2).

[35] The strong influence of the plasma resonance is in agreement with the 2004 results [*Kosch et al.*, 2005; *Mishin et al.*, 2005a], where I(6300) doubled at the plasma resonance and when $f_oF2 \rightarrow 2f_C$ (H_{foF2}). This suggests that L waves participate in electron acceleration at altitudes above H_{UHR}, consistent with the MUIR radar observations of pump-enhanced L waves (Figure 1f). The larger values of the relative optical gain and smaller ultimate intensities reported here, compared to 2004, are probably due to the shorter pump pulses used here (1 min versus 2.5 min in 2004), emphasizing the importance of the initial modification phase within the pumped volume [e.g., *Mishin et al.*, 2004].

[36] The oscillating two-stream instability of L waves ($OTSI_L$) mechanism produces Langmuir waves evolving into strong Langmuir turbulence, which has a typical radar signature, i.e., the central peak in the ion-line incoherent scatter spectrum [e.g., *DuBois et al.*, 1993]. Unfortunately, such data are not available for our experiment. However, we expect that the $OTSI_L$ mechanism was not active because the strict frequency matching condition was not met because of pumping outside the Spitze cone, the low pump power (~11 MW ERP) used makes stimulating $OTSI_L$ unlikely, and no optical emissions were observed at the poleward edge of the pump beam which happens to be inside the Spitze cone. Hence in the following discussion on Langmuir turbulence, we focus on the weak turbulence PDI_L mechanism.

[37] Since the zenith angle of the magnetic field (χ) at HAARP is small (~15°), a substantial component of the pump wave electric field is parallel to the magnetic field in the region of downward reflection [*Mishin et al.*, 2001]. Thus the generation of weak Langmuir turbulence by the pump wave for oblique incidence should be similar to that for the vertical incidence. For vertical incidence, a standing wave is created near reflection, the so-called Airy pattern. Pumping in the MZ does not create an Airy

pattern because of the oblique incidence, which causes the reflected wave to propagate away. Hence the effect of inhomogeneity, which increases the damping rate [e.g., *Fejer*, 1979], is insignificant in the MZ. We evaluate the critical angle of incidence beyond which classical PDI_L is not possible. The PDI_L matching conditions are: $\omega_O \simeq \omega_P^2\sqrt{1+3k_L^2r_D^2\cos^2\theta+\omega_C^2/\omega_P\cdot\sin^2\theta} \gg \omega_{IA}$ and $k_L \simeq k_{IA}$, where k_L and k_{IA} are the wave numbers of the Langmuir and ion-acoustic electrostatic waves, respectively, $k_{L\|} = k_L \cos\theta = \sqrt{k_L^2 - k_{L\perp}^2}$, and $r_D \sim 1$ cm is the Debye radius ($k_L \gg \omega_O/c$ is assumed). At the reflection altitude (H_O), $\omega_P \simeq \omega_O \cos\chi$, where χ is the magnetic zenith angle, and the first of the matching conditions for $\theta \to 0$ is fulfilled at $k_L \simeq r_D \tan\chi/\sqrt{3}$. Comparing the Landau damping rate γ_L with the collisional rate $\nu_e/2$, one finds that for a broad range of F-region plasma parameters, $\gamma_L < \nu_e/2$ so long as $\chi < 17°$. Therefore the well-known features of PDI_L for vertical pump wave injections [e.g., *Fejer*, 1979] are also valid for MZ pump wave injections atHAARP and EISCAT, where the magnetic zenith angles are ~15° and ~13°, respectively, i.e., <17°. This is consistent with radar observations by *Isham et al.* [1999], *Dhillon and Robinson* [2005], *Ashrafi et al.* [2007], *Oyama et al.* [2006], and the MUIR observations presented here. The corollary to the above is that PDI_L cannot be stimulated in the magnetic zenith at lower latitude ionospheric pumping facilities, i.e., for $\chi > 17°$, because of increased Landau damping.

[38] Figure 1 shows no apparent change in the optical emission intensity during the double resonance crossing (~03:45 UT, label 4). At first glance, this suggests that within 1 min, the TPI_{UH} (striations)-related processes did not develop sufficiently to contribute to the electron heating/acceleration process. However, the MUIR plasma-line overshoot-like behavior after ~03:45 UT indicates that PDI_L development is quickly suppressed, most likely due to striation-related anomalous absorption [e.g., *Stubbe et al.*, 1994]. This is consistent with the pump-induced SuperDARN radar backscatter power enhancements almost doubling in amplitude after ~03:45 UT. Thus we conclude that the TPI_{UH} mechanism's contribution (UH waves) to the optical emission intensity is comparable to that from the PDI_L mechanism (L waves). However, we note that the $I(6300)$ and $I(5577)$ increases and decreases, respectively, after ~03:45 UT. This suggests that the energy spectrum of the accelerated electrons is softening, contrary to the study of *Kosch et al.* [2005]. Unfortunately, this can not be checked quantitatively with the present data set as the pump pulses were too short to ensure that $I(6300)$ reached the steady state.

[39] The dispersion equation, i.e., the dielectric permittivity ($\varepsilon_\perp$) = 0, for $k_\| \ll k_\perp$ and $x = k_\perp^2 r_C^2 \ll 1$ ($r_C \simeq 3$ cm is the gyroradius of the thermal electrons) [e.g., *Ichimaru*, 1973] is:

$$\varepsilon_\perp(\omega,k) = \frac{\omega^2-\omega_{UHR}^2}{\omega^2-\omega_C^2} - \frac{3\omega_P^2\omega_C^2 x}{(\omega^2-\omega_C^2)(\omega^2-4\omega_C^2)} = 0 \quad (1)$$

where $\omega = 2\pi f$. From equation (1), the general frequency solution $\delta_{1,2} = \frac{\delta_{UHR}}{2} \pm \sqrt{\frac{\delta_{UHR}^2}{4} + \frac{9}{64}x}$ is readily obtained, where $\delta = \frac{f-2f_C}{2f_C}$ and $\delta_{UHR} = \frac{f_{UHR}-2f_C}{2f_C}$. In the immediate vicinity of $2f_C$, i.e., $\delta_{UHR}^2 \ll \frac{9}{16}x$, one gets $\delta_{1,2}(x) \simeq \frac{\delta_{UHR}}{2} \pm \frac{3}{8}\sqrt{x}$, while at $1 \gg \delta_{UHR}^2 \gg \frac{9}{16}x$, the two frequencies are distinct, namely, $\delta_1(x) \simeq \delta_{UHR} + \frac{9}{64}x/\delta_{UHR}$ and $\delta_2(x) \simeq -\frac{9}{64}x/\delta_{UHR}$ [e.g., *Grach*, 1979]. The UH and EB modes correspond to the positive and negative sign of $\frac{\partial}{\partial x}\delta$, respectively.

[40] Clearly, for $f_O = f_{UHR}(H_{UHR}) < 2f_C(H_{UHR})$, or $\delta_O = \delta_{UHR} < 0$, only matching with EB modes is possible, and thus TPI_{UH} cannot develop [*Mjølhus*, 1993]. Only when the double plasma resonance is reached (after ~03:45 UT in our case) can UH modes exist, and therefore the TPI_{UH} can grow. This is in agreement with the increased amplitude in pump-enhanced SuperDARN radar backscatter and MUIR radar backscatter switching from persistent to overshoot in character at ~03:45 UT (Figure 1, label 4). However, the question remains as to what the cause is for the Kodiak backscatter enhancements prior to ~03:45 UT, when only EB modes appear possible since the HF radar backscatter comes from the striations, which are symbiotic with UH modes only. This issue is addressed later.

[41] The TPI_{UH} threshold near the second GH strongly depends on the frequency mismatch [*Grach*, 1979]:

$$E_{TPI_{UH}} \simeq 0.15\sqrt{\left(\xi_{in}+\kappa_\|^2 l_e^2+\kappa_\perp^2 r_C^2\right)\frac{\partial(\omega^2\varepsilon_\perp)}{\omega\partial\omega}}\left[\frac{V}{m}\right] \quad (2)$$

where $\xi_{in} \sim 10^{-4}$ and $l_e \sim 0.5-1$ km are the coefficient of inelastic losses and mean free path of thermal electrons, respectively, and $1/\kappa_\|$ ($1/\kappa_\perp$) is the longitudinal (transverse) extent of field-aligned density irregularities, $\kappa_\perp \gg \kappa_\|$. This implies that $\kappa_\| \gg \kappa_\|^* = |\nabla_\| n_e|/n_e = 1/L_n$, where $L_n \sim 50$ km is the F-region plasma density gradient scale.

[42] The value of $\frac{\partial(\omega^2\varepsilon_\perp)}{\omega\partial\omega}$ is $\gg 20$ for $|\delta_{UHR}| \gg \frac{3}{4}\kappa_\perp r_C$ and ≈16/3 for $|\delta_{UHR}| \ll \frac{3}{4}\kappa_\perp r_C$ [*Grach*, 1979], so that one expects TPI_{UH} to develop only for $|\delta_{UHR}| < \frac{3}{4}\kappa_\perp r_C$. For the optimum transverse scale of striations $a_m \simeq \left(\frac{f_O}{2f_C}-1\right)^{-\frac{1}{4}}$ m to achieve the nonlinear explosive growth phase [*Vaskov and Gurevich*, 1977; *Gurevich et al.*, 2002], the latter inequality translates into $\delta_{UHR} < \delta_{UHR}^{(m)} \simeq 0.01$ [*Mishin et al.*, 2005a]. From analysis of the frequency-height profiles (see Figure 4), it follows that the latter holds until ~04:34 UT (Figure 1, label 6), after which the growth rate of TPI_{UH} decreases because of the increasing threshold, correlating with the decrease in the pump-induced SuperDARN radar backscatter power around this time.

[43] The free-space electric field of the injected pump wave ($E_O = 5.5\sqrt{P}/r$) is ~75 mV/m at a distance of $r \simeq 250$ km [*Mishin et al.*, 2005b]. For $E_O \sim 75$ mV/m and $x \gg \xi_{in} + \kappa_\|^2 l_e^2$, condition (2) reduces to $E_O > E_{TPI_{UH}} \simeq 0.15\sqrt{\frac{3}{16}\kappa_\perp^2 r_C^2}$ and yields $\kappa_\perp r_C < 0.22$, provided that $|\delta_{UHR}| < 0.1$. The long-scale perturbations, $\kappa_\| l_e \ll \kappa_\perp r_C < \xi_{in}^{-1/2} \sim 10^{-2}$, appear to have a low threshold value of ~15 mV/m, which is less than the injected pump electric field. However, since these waves have $\kappa_\| \ll \kappa_\|^*$, the background inhomogeneity hampers their development [e.g., *Grach*, 1979]. Figure 5 shows dispersion curves of the UH mode waves at the F-layer peak during the latter part of the experiment, when $f_O > 2f_C$ (H_{foF2}) ≥ f_{UHR} (H_{foF2}). At 04:34, 04:45, 04:50, and 04:51 UT, the matching values

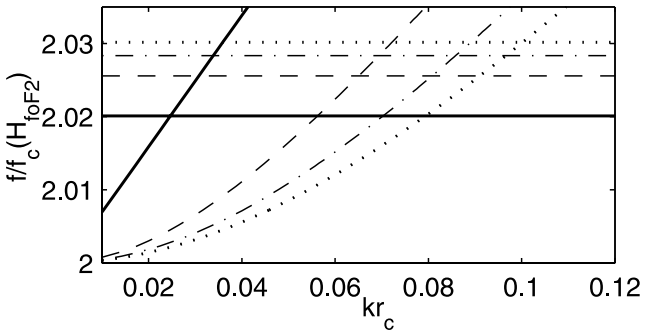

Figure 5. Dispersion curves of the upper-hybrid mode waves at H_{foF2} at 04:34 (solid line), 04:45 (dashed line), 04:50 (dash-dotted line), and 04:51 (dotted line) UT. The corresponding horizontal lines show the ratio f_O/f_C (H_{foF2}).

of $\kappa_\perp r_C$ were 0.028, 0.07, 0.09, and 0.1, respectively, and the values of δ_{UHR} (H_{foF2}) were $\simeq -0.0025$, -0.046, -0.065, and -0.09, respectively. Clearly, after 04:45 UT, $|\delta_{UHR}(H_{foF2})| > \frac{3}{4}\kappa_\perp r_C$, and thus the TPI_{UH} could hardly be excited. This coincides with the abrupt disappearance of the pump-enhanced SuperDARN radar backscatter (Figure 1e, label 7). This result is consistent with the prediction for orthogonal backscatter shown in Figure 3, since the worsening conditions for F-region orthogonal backscatter in a weakening ionosphere is a gradual process and is hardly responsible for such a sudden change. The same is true for TPI_{UH}, which is obviously possible beyond the idealized cutoff time ($\sim$04:34 UT) predicted by the ionosonde data (Figure 1b, label 6).

[44] The threshold of the parametric decay $PDI_{UH/EB}$ near the second GH is [*Mishin et al.*, 2005a]:

$$E^{\nu}_{PDI} \simeq \frac{0.15}{T_e[eV]}\frac{f_O^2[MHz]}{3-\Delta_{LH}}\sqrt{\frac{\Delta_{LH}}{x}\left[\frac{mV}{m}\right]} \qquad (3)$$

where $\Delta^2_{LH} = f^2_{LH}/f^2_{LHR} \simeq 1 + Y^2 + \left(\frac{3}{4} + 3\frac{T_i}{T_e}\right)x$, $Y = \mu^{-1/2}\kappa_\parallel/\kappa$, $f_{LHR} = f_C\mu^{1/2}$ is the lower hybrid resonance (LHR) frequency, and $\mu \approx 3\cdot 10^{-5}$ is the electron-to-ion mass ratio [e.g., *Ichimaru*, 1973]. The superscript ν indicates that collisional damping has been assumed, i.e., $\nu_{LH} \simeq \frac{3}{8}\nu_e$, $\nu_{UH} \simeq \frac{5}{8}\nu_e$, and $\nu_{EB} \simeq \nu_e$ for the LH, UH, and EB modes, respectively [*Istomin and Leyser*, 1995], where ν_e is the electron collision frequency.

[45] From equation (2), it follows that $E_O > E^{\nu}_{PDI}$ as long as $\Delta_{LH} < \sqrt{2}$ and $x_m > 5\cdot 10^{-3}$, where x_m is defined by the matching conditions $f_{1,2}(x) = f_O - f_{LH}$ and $\overrightarrow{k_O} = \overrightarrow{k_{HF}} + \overrightarrow{k_{LH}}$. More generally, the threshold electric field equals $E_{PDI} = E^{\nu}_{PDI}\sqrt{\Gamma_{UH/EB}\Gamma_{LH}/\nu_{UH/EB}\nu_{LH}}$, where $\Gamma_{LH,UH/EB} = \gamma_{LH,UH/EB} + \nu_{LH,UH/EB}$ and $\gamma_{LH,UH/EB}$ is the collisionless damping rate. Collisionless damping of UH/EB waves is negligible, while that for LH waves is [e.g., *Mikhailovskii*, 1974]:

$$\gamma_{LH} \simeq \frac{\omega_{LHR}\sqrt{\frac{\pi/2}{x}}\Delta^2_{LH}}{1-I_O(x)e^{-x}}\left[\frac{T_e}{T_i}\exp\left(-\frac{T_e\Delta^2_{LH}}{2T_i x}\right)\right] + \frac{I_O(x)}{\sqrt{Y}}\exp\left(-x-\frac{\Delta^2_{LH}}{2Y^2x}\right) \qquad (4)$$

where the first and second terms represent the ion and electron Landau damping, respectively, and $I_O(x)$ is the zero-order modified Bessel function.

[46] Figure 6 shows the variation of γ_{LH}/ν_{LH}, the ratio of collisionless to collisional damping, with kr_C for $Y = 1/2$, 1, $\sqrt{2}$, $\sqrt{3}$. Clearly, for $kr_C < 0.2$, the collisionless damping is negligible, and $PDI_{UH/EB}$ should develop as described by *Mishin et al.* [2005a]. Prior to the double-resonance crossing at $\sim$03:45 UT, the most favorable conditions for PDI_{EB} development above H_{UHR} are achieved near the reflection altitude, where $\delta_{UHR} \simeq 0.1$. Assuming $f_O = 2f_C(H_O) - a\cdot f_{LHR}$, then $x_m \simeq \frac{32}{9}(a+1)\mu^{1/2}\delta_{LHR}$ so that condition (2) is fulfilled at $a \geq 1$, where a is an arbitrary number. After the double-resonance crossing at $\sim$03:45 UT, $f_O = 2f_C(H_{UHR}) + a\cdot f_{LHR}$, and PDI_{UH} develops below H_{UHR} at altitudes where $\delta_{UHR} < -\frac{0.25}{a-1} < 0$. For $L_n = 50$ km, $|\delta_{UHR}|$ varies by $\sim$0.009/km, and the latter condition implies $a \geq 2$. Clearly, the PDI_{EB}-created EB modes are close to the cyclotron resonance.

[47] Electron acceleration via cyclotron resonance $v_\parallel = \frac{\omega_k - 2\omega_C}{k_\parallel}$ enhances when $\omega_k \to 2\omega_C$. Acceleration of the background suprathermal electron population (i.e., photoelectrons) provides many more "seed" electrons than are available from the ionospheric thermal population [*Mishin and Telegin*, 1986; *Grach*, 1999; *Mishin et al.*, 2004]. For suprathermal electrons with $\frac{mv_\parallel^2}{2} = 1 - 10$ eV and $k_\parallel \sim \frac{2\pi f_O}{c}$, the magnitude of the frequency mismatch $\Delta f = f(k) - 2f_C$ should not exceed an upper limit of $\Delta f_\# \simeq (0.3-1)10^{-2} f_O \sim 10 - 30$ kHz or $(1.2-3.6)f_{LHR}$. At $\sim$04:14 UT, this limit was exceeded for the F-layer peak, i.e., $f_oF2 - 2f_C(H_{foF2}) \approx -35$ kHz. Note that this does not necessarily mean that electron acceleration is no longer possible. Above the F-layer peak, the longitudinal wave vectors $k_\parallel$ of upward-propagating waves increases so that the cyclotron resonance is still possible. However, since the wave energy is reduced by collisional damping, the acceleration efficiency decreases; consistent with the $I(5577)$ behavior (Figure 1d).

[48] The solid diagonal line in Figure 1b gives the solar terminator altitude. It intersected with the reflection altitude after $\sim$04:06 UT so that the photoelectrons at and below H_O became available only via transport from above. We calculate the spatial rate of suprathermal electron energy loss for

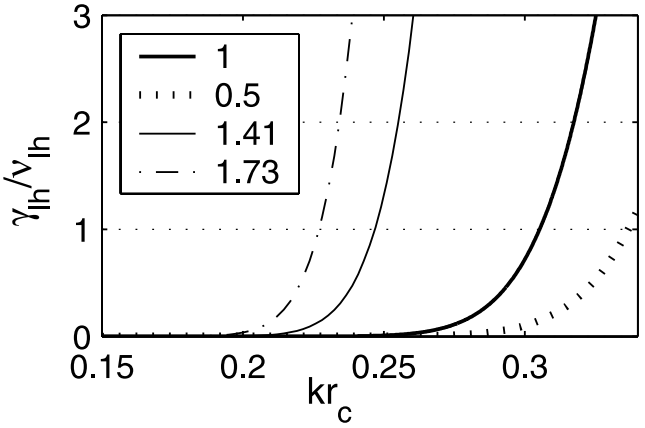

Figure 6. The variation of collisionless-to-collisional damping (γ_{LH}/ν_{LH}) with kr_c at $Y = 0.5$, 1, $\sqrt{2}$, and $\sqrt{3}$.

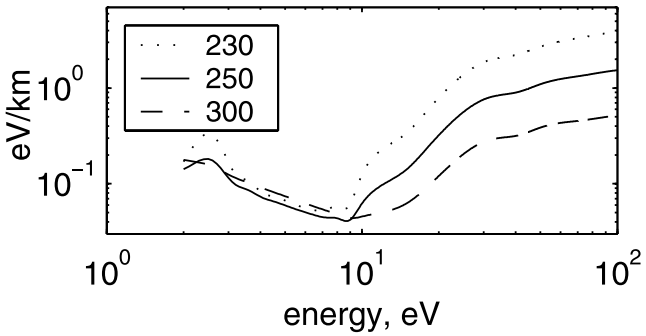

Figure 7. The energy loss rate (in eV/km) of suprathermal electrons at altitudes of 230 (dotted), 250 (solid), and 300 (dashed) km.

different altitudes, shown in Figure 7. Clearly, for the low-energy electrons, it is hard to make it to the acceleration region at lower altitudes, and thus the contribution of the suprathermal population to $I(6300)$ should decrease. This is consistent with the abrupt decrease in the red line intensity by ~30% at ~04:09 UT. On the other hand, $\geq$10 eV electrons appear capable of reaching H_O and even H_{UHR} [e.g., *Bernhardt et al.*, 1989] to participate in the pump-induced acceleration process, contributing mainly to $I(5577)$. This explains why $I(5577)$ hardly varies, while $I(6300)$ drops significantly at ~04:09 UT.

[49] The gradual variation in the artificial optical intensities during 03:40–04:10 UT is now addressed. The volume emission rate of $I(6300)$, VER(6300), is mainly determined by the electron temperature altitude profile [e.g., *Mantas and Carlson*, 1996; *Mishin et al.*, 2004]. VER(6300) is very sensitive to the energy distribution of the thermal electrons, which may deviate significantly from a Maxwellian distribution because of inelastic collisions with molecular nitrogen (N_2) [*Mishin et al.*, 2000]. For a given plasma density n_e, this deviation decreases with altitude as the N_2 density decreases, likewise the collisional deactivation of the $O(^1D)$ state. Both effects provide for an increasing VER(T_e) during the course of twilight observations [*Mishin et al.*, 2000, 2004]. Thus following H_{foF2}, $I(6300)$ is expected to rise when H_O approaches H_{foF2} or $f_oF2 \rightarrow f_P$ (H_O). On the other hand, the $O(^1S)$ emission is dominated by suprathermal electrons and increases for lower altitudes. Therefore $I(5577)$ is expected to decrease when f_oF2 approaches $f_P(H_O)$. Both these conjectures agree well with the data (Figures 1c and 1d) [cf. *Mishin et al.*, 2005b].

[50] Assuming that we always approach important frequency boundaries from below, we have established that prior to plasma resonance at ~03:37 UT (Figure 1, label 3), the PDI_L and PDI_{EB} mechanisms were operational, and this probably continued until double resonance at ~03:45 UT (Figure 1, label 4) but with increased efficiency. Unfortunately, the limited data set between plasma and double resonance, coupled to Digisonde and MUIR radar data gaps, makes for some uncertainty in this small interval. After double resonance and prior to the cessation of nominal HF reflection at ~04:12 UT (Figure 1, label 5), the TPI_{UH} and PDI_{UH} mechanisms were operational, with PDI_L being only present at the start of the pump pulse because of the growth of striations. After the cessation of HF reflection, i.e., an underdense ionosphere, the TPI_{UH} and PDI_{UH} mechanisms were operational without the presence of PDI_L.

[51] The presence of pump-induced HF radar backscatter (Figure 1e) after double resonance (~03:45 UT, label 4) is easily understood since the TPI_{UH} mechanism is symbiotic with meter-scale plasma irregularities (striations), which result in backscatter if the orthogonality condition is met (Figure 3). However, prior to double resonance, when only PDI_L and PDI_{EB} were present, the SuperDARN radar also observed pump-induced backscatter enhancements. PDI_L is $EM_O \rightarrow L + IA$, producing waves near parallel to the magnetic field directions to which the side-viewing HF radar is insensitive. PDI_{EB} is $EM_O \rightarrow EB + LH$. EB waves would be trapped by field-aligned plasma enhancements. *Istomin and Leyser* [1997] pointed out that increasing electron temperature in a region of short transverse scale ($l_\perp < 3$ m) leads to electron motion into this region, so that the plasma density increases, unlike for $l_\perp > 3$ m. This may establish a positive feedback loop between EB wave heating and plasma enhancements, leading to an instability [*Huang et al.*, 1995], just like UH wave heating and striations. However, short transverse scales are not favorable for 8 MHz backscatter, the Bragg scatter condition is $l_\perp \approx$ 19 m. Ionospheric topside rocket measurements found natural LH wave-density depletions with a transverse scale size of $l_\perp \approx 20$ m [*Vago et al.*, 1992], almost exactly that required for HF backscatter. LH wave density cavitons generated via EB + LH $\rightarrow$ EM can undergo collapse [*Musher et al.*, 1978; *Mishin et al.*, 2004], which results in electron acceleration and hence artificial optical emissions. Hence we conclude that the SuperDARN HF radar backscatter is the result of pump-induced LH wave density cavitons. This is the first identification of SuperDARN radar backscatter from cavitons associated with LH waves.

[52] *Djuth et al.* [2005] published SEE spectra for ionospheric pumping below the second GH, showing the DM feature. However, for the pump-frequency regime used, only EB and LH plasma waves could have been present. This excludes the TPI_{UH} mechanism, meaning that the UH wave-associated striations were not present, which are an essential feature for producing the SEE [*Carozzi et al.*, 2002]. We have already shown that density enhancements associated with EB waves are unlikely. Hence it seems likely that the density depletions necessary for generating SEE are produced by the LH cavitons, i.e., the field-aligned density cavity is created by the LH wave ponderomotive force. In this scenario, the SEE spectra by *Djuth et al.* [2005] are entirely consistent with the SuperDARN radar observations of LH cavitons, reported here for the first time.

4. Conclusion

[53] During an ionospheric pumping experiment at HAARP, a frequency pass from below to above the second electron gyroharmonic was executed. Simultaneous HF and UHF radar observations and multiwavelength optical observations were performed. These observations are consistent with the coexistence of the parametric decay and thermal parametric instabilities just above the second gyroharmonic. Two, sometimes three, mechanisms operate simultaneously

for long pump pulses, thereby explaining the variations in artificial optical emission intensity.

[54] Theoretically, radio wave parametric decay into Langmuir and ion-acoustic plasma waves is only possible while reflection is nominally possible, i.e., within the Spitze cone, because of the required frequency-matching condition. This mechanism is shown to be possible for injection zenith angles up to $\sim 17^\circ$, i.e., well outside the Spitze cone at high latitudes. Hence parametric decay into Langmuir and ion-acoustic waves is possible while pumping into the magnetic zenith at high-latitude sites such as HAARP and EISCAT.

[55] Pump wave parametric decay into electron Bernstein (upper-hybrid) and lower-hybrid plasma waves occurs for pump frequencies below (above) the second gyroharmonic only. The thermal parametric instability, which produces upper-hybrid waves on plasma irregularities, only operates above the second gyroharmonic frequency and accounts for the observed HF radar backscatter asymmetry. The fact that upper-hybrid waves and striations are impossible for pump frequencies below the second gyroharmonic, and the improbability of electron-Bernstein wave trapping in plasma enhancements of a transverse scale size necessary to meet the radar backscatter Bragg condition, means that the Super-DARN radar centerline observations of enhanced backscatter in this regime are due to lower-hybrid wave cavitons. This is the first time such radar observations, associated with pump-enhanced lower-hybrid waves in the ionosphere, have been identified and reported.

[56] Two areas for further investigation are the accelerated electron energy spectrum, which may be different for different frequency regimes about the second gyroharmonic, and details of what happens between the closely spaced plasma and double-resonance frequencies.

[57] **Acknowledgments.** The authors thank the following persons for their invaluable contributions: L. Snyder for setting up a fast-sweeping Digisonde mode synchronized to HAARP, permitting real-time determination of the correct pump frequency to find the second gyrofrequency. M. McCarrick for operating the HAARP facility. R. Esposito for upgrading the HAARP all-sky imager to improve its sensitivity. The HAARP program is a Department of Defense project managed jointly by the US Air Force and US Navy. This research was supported in part by AFRL contract F19628-02-C-0087 with Boston College and AFOSR under tasks 2311SD and 2311AS. M.J.K acknowledges support by the National Research Council Research Associateship program.

[58] Wolfgang Baumjohann thanks Spencer Kuo and another reviewer for their assistance in evaluating this paper.

References

Ashrafi, M., M. J. Kosch, and F. Honary (2006), Heater-induced altitude descent of the EISCAT UHF ion-line overshoot: Observations and modeling, *Adv. Space Res.*, *38*, 2645–2652.

Ashrafi, M., M. J. Kosch, K. Kaila, and B. Isham (2007), Spatio-temporal evolution of HF-induced artificial optical emissions, radar backscatter and Stimulated Electromagnetic Emissions at EISCAT, *J. Geophys. Res.*, *112*, A05314, doi:10.1029/2006JA011938.

Bernhardt, P., C. Tepley, and L. Duncan (1989), Airglow enhancements associated with plasma cavities formed during ionospheric heating experiments, *J. Geophys. Res.*, *94*, 9071–9092.

Brändström, B. U. E., T. B. Leyser, A. Steen, M. T. Rietveld, B. Gustavsson, T. Aso, and M. Ejiri (1999), Unambiguous evidence of HF pump-enhanced airglow at auroral latitudes, *Geophys. Res. Lett.*, *26*, 3561–3564.

Carozzi, T. D., B. Thide, S. M. Grach, T. B. Leyser, M. Holz, G. P. Komrakov, V. L. Frolov, and E. N. Sergeev (2002), Stimulated electromagnetic emissions during pump frequency sweep through fourth electron cyclotron harmonic, *J. Geophys. Res.*, *107*(A9), 1253, doi:10.1029/2001JA005082.

Das, A. C., and J. A. Fejer (1979), Resonance instability of small-scale field-aligned irregularities, *J. Geophys. Res.*, *84*, 6701–6704.

Dhillon, R. S., and T. R. Robinson (2005), Observations of time dependence and aspect sensitivity of regions of enhanced UHF backscatter associated with RF heating, *Ann. Geophys.*, *23*, 75–85.

Djuth, F. T., B. Isham, M. T. Rietveld, T. Hagfors, and C. LaHoz (2004), The first one hundred milliseconds of HF modification at Tromsø, Norway, *J. Geophys. Res.*, *109*, A11307, doi:10.1029/2003JA010236.

Djuth, F. T., T. R. Pedersen, E. A. Gerken, P. Bernhardt, C. A. Selcher, W. A. Bristow, and M. J. Kosch (2005), Ionospheric modification at twice the electron cyclotron frequency, *Phys. Rev. Lett.*, *94*, 125001.

DuBois, D. F., A. Hanssen, H. A. Rose, and D. Russell (1993), Space and time distribution of HF excited Langmuir turbulence in the ionosphere: Comparison of theory and experiment, *J. Geophys. Res.*, *98*, 17,543–17,567.

Dysthe, K. B., E. Mjølhus, H. Pecséli, and K. Rypdal (1982), Thermal cavitons, *Phys. Scr.*, *T2/2*, 548–559.

Fejer, J. (1979), Ionospheric modification and parametric instabilities, *Rev. Geophys.*, *17*, 135–153.

Fejer, A. J., and E. Leer (1972), Excitation of parametric instabilities by radio waves in the ionosphere, *Radio Sci.*, *7*, 481–491.

Fialer, P. A. (1974), Field-aligned scattering from a heated region of the ionosphere—Observations at HF and VHF, *Radio Sci.*, *9*, 923–940.

Grach, S. M. (1979), Thermal parametric instability in ionospheric plasma at frequencies close to ω_{He} and $2\omega_{He}$, *Radiophys. Quantum Electron.*, *22*, 357–363.

Grach, S. M., N. A. Mityakov, V. O. Rapoport, and V. Yu. Trakhtengertz (1981), Thermal parametric turbulence in a plasma, *Physica D (Amsterdam)*, *2*, 102–106.

Grach, S. M. (1999), On kinetic effects in the ionospheric F-region modified by powerful radio waves, *Radiofizika*, *42*(7), 651–669.

Grach, S. M., B. Thide, and T. B. Leyser (1994), Plasma waves near the double resonance layer in the ionosphere, *Radiophys. Quantum Electron.*, *37*, 392–402.

Gurevich, A. V., H. Carlson, M. Kelley, T. Hagfors, A. Karashtin, and K. P. Zybin (1999), Nonlinear structuring of the ionosphere modified by powerful radio waves at low latitudes, *Phys. Lett. A*, *251*, 311–321.

Gurevich, A. V., K. P. Zybin, H. C. Carlson, and T. Pedersen (2002), Magnetic zenith effect in ionospheric modifications, *Phys. Lett. A*, *305*, 264–274.

Gustavsson, B., et al. (2001), First tomographic estimate of volume distribution of HF-pump enhanced airglow emission, *J. Geophys. Res.*, *106*, 29,105–29,124.

Gustavsson, B., B. U. E. Brändström, A. Steen, T. Sergienko, T. B. Leyser, M. T. Rietveld, T. Aso, and M. Ejiri (2002), Nearly simultaneous images of HF-pump enhanced airglow at 6300 A and 5577 A, *Geophys. Res. Lett.*, *29*(24), 2220, doi:10.1029/2002GL015350.

Gustavsson, B., et al. (2005), The electron distribution during HF pumping, a picture painted with all colors, *Ann. Geophys.*, *23*, 1747–1754.

Gustavsson, B., T. B. Leyser, M. J. Kosch, M. T. Rietveld, A. Steen, B. U. E. Brändström, and T. Aso (2006), Electron gyroharmonic effects in ionization and electron acceleration during HF pumping in the ionosphere, in revision, *Phys. Rev. Lett*.

Haslett, J. C., and L. R. Megill (1974), A model of the enhanced airglow excited by RF radiation, *Radio Sci.*, *9*, 1005–1019.

Honary, F., A. J. Stocker, T. R. Robinson, T. B. Jones, and P. Stubbe (1995), Ionospheric plasma response to HF radio waves operating at frequencies close to the third harmonic of the electron gyrofrequency, *J. Geophys. Res.*, *100*, 21,489–21,501.

Honary, F., T. R. Robinson, D. M. Wright, A. J. Stocker, M. T. Rietveld, and I. McCrea (1999), First direct observations of the reduced striations at pump frequencies close to the electron gyroharmonics, *Ann. Geophys.*, *17*, 1235–1238.

Huang, J., and S. Kuo (1994), A theoretical model for the broad upshifted maximum in the stimulated electromagnetic emission spectrum, *J. Geophys. Res.*, *99*, 19,569–19,576.

Huang, J., S. Kuo, and H. Zhou (1995), A theoretical study on the broad symmetric structure in the simulated electromagnetic emission spectrum, *J. Geophys. Res.*, *100*, 1639–1645.

Hughes, J. M., W. A. Bristow, R. T. Parris, and E. Lundell (2003), SuperDARN observations of ionospheric heater-induced upper hybrid waves, *Geophys. Res. Lett.*, *30*(24), 2276, doi:10.1029/2003GL018772.

Hughes, J. M., W. A. Bristow, and R. T. Parris (2004), SuperDARN observations of spectral enhancements excited during an ionospheric heating experiment, *Geophys. Res. Lett.*, *31*, L08808, doi:10.1029/2004GL019613.

Ichimaru, S. (1973), *Basic Principles in Plasma Physics: A Statistical Approach*, Addison-Wesley, Boston, Mass.

Isham, B., T. Hagfors, E. Mishin, M. T. Rietveld, C. La Hoz, W. Kofman, and T. Leyser (1999), A search of the HF excitation of enhanced ion

acoustic and Langmuir waves with EISCAT and the Tromsø heater, *Radiophys. Quantum Electron.*, *42*, 607–618.
Istomin, Ya. N., and T. B. Leyser (1995), Parametric decay of an electromagnetic wave near electron cyclotron harmonics, *Phys. Plasmas*, *2*, 2084–2097.
Istomin, Ya. N., and T. B. Leyser (1997), Small-scale magnetic field-aligned density irregularities excited by a powerful electromagnetic wave, *Phys. Plasmas*, *4*, 817–828.
Istomin, Ya. N., and T. B. Leyser (1998), Parametric interaction of self-localized upper hybrid states in quantized plasma density irregularities, *Phys. Plasmas*, *5*, 921–931.
Istomin, Ya. N., and T. B. Leyser (2003), Electron acceleration by cylindrical upper hybrid oscillations trapped in density irregularities in the ionosphere, *Phys. Plasmas*, *10*, 2962–2970.
Kjus, S. H., H. L. Pécseli, B. Lybekk, J. Holtet, J. Trulsen, H. Lühr, and A. Eriksson (1998), Statistics of the lower hybrid wave cavities detected by the FREJA satellite, *J. Geophys. Res.*, *103*, 26,633–26,647.
Kosch, M. J., M. T. Rietveld, T. K. Yeoman, K. Cierpka, and T. Hagfors (2002a), The high-latitude artificial aurora of 21 February 1999: An analysis, *Adv. Polar Upper Atmos. Res*, *16*, 1–12.
Kosch, M. J., M. T. Rietveld, A. J. Kavanagh, C. Davis, T. Yeoman, F. Honary, and T. Hagfors (2002b), High-latitude pump-induced optical emissions for frequencies close to the third electron gyro-harmonic, *Geophys. Res. Lett.*, *29*(23), 2112, doi:10.1029/2002GL015744.
Kosch, M. J., M. T. Rietveld, A. Senior, I. W. McCrea, A. J. Kavanagh, B. Isham, and F. Honary (2004), Novel artificial optical annular structures in the high latitude ionosphere, *Geophys. Res. Lett.*, *31*, L12805, doi:10.1029/2004GL019713.
Kosch, M. J., T. Pedersen, J. Hughes, R. Marshall, E. Gerken, A. Senior, D. Sentman, M. McCarrick, and F. Djuth (2005), Artificial optical emissions at HAARP for pump frequencies near the third and second gyroharmonic, *Ann. Geophys.*, *23*, 1585–1592.
Kosch, M. J., T. Pedersen, E. Mishin, M. Starks, E. Gerken-Kendall, D. Sentman, S.-I. Oyama, and B. Watkins (2007), Temporal evolution of pump beam self-focusing at HAARP, *J. Geophys. Res.*, doi:10.1029/2007JA012264, in press.
Kuo, S., and M. Rubinraut (2005), Generation of energetic electrons at second harmonic cyclotron resonance in ionospheric HF heating experiments, *Geophys. Res. Lett.*, *32*, L19102, doi:10.1029/2005GL023186.
Kuo, S., M. Lee, and P. Kossey (1997), Excitation of oscillating two stream instability by upper hybrid pump in ionospheric heating experiments at Tromsø, *Geophys. Res. Lett.*, *24*, 2969–2972.
Leyser, T. (2001), Stimulated electromagnetic emissions by high-frequency electromagnetic pumping of the ionospheric plasma, *Space Sci. Rev.*, *98*, 223–328.
Mantas, G. P., H. C. Carlson (1996), Reinterpretation of the 6300-Å airglow enhancements observed in ionosphere heating experiments based on analysis of Platteville, Colorado, data, *J. Geophys. Res.*, *101*, 195–210.
Mikhailovskii, A. B. (1974), Instabilities of a homogenous plasma in *The Theory of Plasma Instabilities*, vol. 1, Consult. Bur., New York, USA.
Minkoff, J., P. Kugelman, and J. Weissman (1974), Radio frequency scattering from a heated ionospheric volume, 1, VHF/UHF field-aligned and plasma line backscatter measurements, *Radio Sci.*, *9*, 941–955.
Mishin, E., and V. Telegin (1986), Spectrum of suprathermal electrons in the auroral plasma, *Sov. J. Plasma Phys.*, *12*, 509–511.
Mishin, E., H. C. Carlson, and T. Hagfors (2000), On the electron distribution function in the F region and Airglow enhancements during HF modification experiments, *Geophys. Res. Lett.*, *18*, 2857–2860, doi:10.1029/2000GL000075.
Mishin, E. T. Hagfors, and B. Isham (2001), A generation mechanism for topside enhanced incoherent backscatter during high frequency modification experiments in Tromsø, *Geophys. Res. Lett.*, *28*, 479–482.
Mishin, E. V., W. J. Burke, and T. Pedersen (2004), On the onset of HF-induced airglow at HAARP, *J. Geophys. Res.*, *109*, A02305, doi:10.1029/2003JA010205.
Mishin, E., M. J. Kosch, T. Pedersen, and W. J. Burke (2005a), HF-induced airglow at magnetic zenith: Coexistence of the thermal and parametric instabilities near electron gyroharmonics, *Geophys. Res. Lett.*, *32*, L23106, doi:10.1029/2005GL023864.
Mishin, E. V., W. J. Burke, and T. Pedersen (2005b), HF-induced airglow at magnetic zenith: Theoretical considerations, *Ann. Geophys.*, *23*, 47–53.
Mjølhus, E. (1993), On the small scale striation effect in ionospheric radio modification experiments near harmonics of the electron gyro frequency, *J. Atmos. Terr. Phys.*, *55*, 907–918.
Musher, S. L., A. M. Rubenchik, and B. I. Sturman (1978), Collective effects associated with lower hybrid heating of plasma, *Plasma Phys.*, *20*, 1131–1150.
Norin, L., S. M. Grach, and B. Thide (2006), On the linear stage of thermal parametric instabilities in the ionosphere excited by HF pumping near electron gyroharmonics, *Adv. Space Res.*, *38*, 2527–2532.
Oyama, S.-I., B. Watkins, F. T. Djuth, M. J. Kosch, P. Bernhardt, and C. J. Heinselman (2006), Persistent enhancement of the HF pump-induced plasma line measured with a UHF diagnostic radar at HAARP, *J. Geophys. Res.*, *11*, A06309, doi:10.1029/2005JA011363.
Pedersen, T. R., and H. C. Carlson (2001), First observations of HF heater-produced airglow at the High Frequency Active Auroral Research Program facility: Thermal excitation and spatial structuring, *Radio Sci.*, *36*, 1013–1026.
Pedersen, T. R., M. McCarrick, E. Gerken, C. Selcher, D. Sentman, H. C. Carlson, and A. Gurevich (2003), Magnetic zenith enhancement of HF radio-induced airglow production at HAARP, *Geophys. Res. Lett.*, *30*(4), 1169, doi:10.1029/2002GL016096.
Ponomarenko, P. V., T. B. Leyser, and B. Thidé (1999), New electron gyroharmonic effects in the HF scatter from pump-excited magnetic field-aligned ionospheric irregularities, *J. Geophys. Res.*, *104*, 10,081–10,087.
Rietveld, M. T., M. J. Kosch, N. R. Blagoveshchenskaya, V. A. Kornienko, T. B. Leyser, and T. K. Yeoman (2003), Ionospheric electron heating, optical emissions and striations induced by powerful HF radio waves at high latitudes: Aspect angle dependence, *J. Geophys. Res.*, *108*(A4), 1141, doi:10.1029/2002JA009543.
Robinson, P. A., A. Melatos, and W. Rozmus (1996a), Is there lower hybrid wave collapse at auroral latitudes?: Theory versus observations, *J. Geophys. Res.*, *101*, 21,545–21,552.
Robinson, T. R., F. Honary, A. J. Stocker, T. B. Jones, and P. Stubbe (1996b), First EISCAT observations of the modification of F-region electron temperatures during RF heating at harmonics of the electron gyro frequency, *J. Atmos. Terr. Phys.*, *58*, 385–3395.
Samara, M., J. LaBelle, C. A. Kletzing, and S. R. Bounds (2004), Rocket observations of structured upper hybrid waves at $f_{uh} = 2f_{ce}$, *Geophys. Res. Lett.*, *31*, L22804, doi:10.1029/2004GL021043.
Sipler, D. P., and M. A. Biondi (1972), Measurements of O(1D) quenching rate in the F region, *J. Geophys. Res.*, *77*, 6202–6212.
Stubbe, P. (1996), Review of ionospheric modification experiments at Tromsø, *J. Atmos. Terr. Phys.*, *58*, 349–368.
Stubbe, P., J. A. Stocker, F. Honary, T. R. Robinson, and T. B. Jones (1994), Simulated electromagnetic emissions and anomalous HF wave absorption near electron gyroharmonies, *J. Geophys. Res.*, *99*, 6233–6246.
Vago, J. L., P. M. Kintner, S. W. Chesney, R. L. Arnoldy, K. A. Lynch, T. E. Moore, and C. J. Pollock (1992), Transverse ion acceleration by localized lower hybrid waves in the topside auroral ionosphere, *J. Geophys. Res.*, *97*, 16,935–16,957.
Vaskov, V. V., and A. V. Gurevich (1977), Resonance instability of small scale plasma perturbations, *J. Exp. Theo. Phys. (Engl. Trans.)*, *46*, 487–494.
Wright, D. M., J. A. Davies, T. K. Yeoman, T. R. Robinson, and H. Shergill (2006), Saturation and hysteresis effects in ionospheric modification experiments observed by the CUTLASS and EISCAT radars, *Ann. Geophys.*, *24*, 543–553.

B. Bristow, S. Oyama, and B. Watkins, Geophysical Institute, University of Alaska, Fairbanks, AK, USA.
J. Hughes, Physical Sciences, Embry-Riddle Aeronautical University, Daytona Beach, FL, USA.
M. J. Kosch and T. Pedersen, Space Vehicles Directorate, Air Force Research Laboratory, Hanscom AFB, Bedford, MA, USA. (m.kosch@lancaster. ac.uk)
E. Mishin, Institute for Scientific Research, Boston College, Chestnut Hill, MA, USA.
A. Senior, Department of Communication Systems, Lancaster University, Infolab21, South Drive, Lancaster, Lancashire, LA1 4WA, UK.